Arabian Journal of Chemistry (2023) **16**, 105161

King Saud University

Arabian Journal of Chemistry

www.ksu.edu.sa
www.sciencedirect.com

Analysis of inclined magnetized unsteady cross nanofluid with buoyancy effects and energy loss past over a coated disk

Shahzeb Khan [a], Assad Ayub [b,c], Syed Zahir Hussain Shah [b], Zulqurnain Sabir [b,d], Amjid Rashid [e], Muhammad Shoaib [f], R. Sadat [g], Mohamed R. Ali [h,i,*]

[a] *Central South University, Changsha, China*
[b] *Department of Mathematics & Statistics, Hazara University, Manshera 21300, Pakistan*
[c] *Department of Mathematics, Government college Mansehra, 21300, Pakistan*
[d] *Department of Computer Science and Mathematics, Lebanese American University, Beirut, Lebanon*
[e] *Department of Mathematics, Abdul Wali Khan University, Mardan, 23200, Khyber Pakhtunkhwa, Pakistan*
[f] *Yuan Ze University, AI Centre, Taoyuan 320, Taiwan*
[g] *Department of Mathematics, Zagazig Faculty of Engineering, Zagazig University, Egypt*
[h] *Faculty of Engineering and Technology, Future University in Egypt, New Cairo 11835, Egypt*
[i] *Basic Engineering Science Department, Benha Faculty of Engineering, Benha University, Banha, Egypt*

Received 21 February 2023; accepted 9 July 2023
Available online 11 July 2023

KEYWORDS

Inclined magnetized environment;
Unsteady Cross fluid;
Buoyancy effects;
Coated disk;
Numerical solutions

Abstract The current study presents an analysis of an inclined magnetized unsteady Cross fluid flowing over a coated disk with buoyancy effects and energy loss. The flow is modeled using the Navier-Stokes equations, including buoyancy, magnetic field, and energy loss effects based on the coated disk. The governing equations are solved numerically by applying the process of bvp4c to analyze the effects of inclination angle, magnetic field strength, and coating thickness using the flow characteristics. The results indicate that the buoyancy effects have a significant impact on the flow along with the results of flow velocity increment along with static pressure decrement. The magnetic field also has significant effects on the flow, which shows the decreasing velocity by increasing the magnetic field. Additionally, the coating thickness has significant effects on energy loss that decrease by increasing the coating thickness. The purpose of this work is to provide the

* Corresponding author.
E-mail address: mohamed.reda@fue.edu.eg (M.R. Ali).
Peer review under responsibility of King Saud University.

Production and hosting by Elsevier

https://doi.org/10.1016/j.arabjc.2023.105161

valuable insight using the buoyancy, magnetic field, and coating thickness effects on the flow characteristics and energy loss based on the inclined magnetic unsteady cross flow passing over a coated disk.

1. Introduction

The magnetic influences present the moving electric charges, magnetic materials, and electric currents. A force perpendicular to the magnetic field and its own velocity always acting as a moving charge in the process of magnetic field, especially in the electromechanics, electrical and engineering magnetic fields that are utilized in all areas of technology. Rotating magnetic field is used in the process of electric motors and power generators. Acharya (Acharya, 2021) examined the effects of nanoparticle on the ferrofluid fluid flow past over a slick rotating disc with oscillating magnetic field. Shailendra (Dandapat and Singh, 2015) investigated two-layer film flow over a non-uniformly spinning disc with attached magnetic field. Hu et al. (Hu et al., 2020) examined the velocity of a disk-shaped micromotor that is influenced by the chemical reaction dependence, magnetic field effects, and surfactant effects. Ray and Dandapat (Ray and Dandapat, 1994) worked on a thin conductive liquid coating associating constant magnetic field. Few multiple studies related to magnetic field attached with several facts, like magnetic forces in the ionized plasma, drug delivery of nano-liposomes and microbubbles with magnetic nanoparticles, and incompressible viscous fluid flow and heat transfer (Dickey et al., 2022; Alishiri et al., 2021; Shuaib et al., 2020).

There are primarily two types of slips in the fluid dynamics, velocity, and the temperature slip. Slip velocity shows the difference between the conveying fluid velocity that is used to convey the particles. The concepts of velocity slip have various applications in the aerodynamic heating, polymer processing, hot rolling, paper production, petroleum industry and coating. Naveed et al. (Naveed Khan et al., 2022) conducted the numerical investigations of the hybrid nanofluid that contains a gyrotactic microbe and numerous slip circumstances. Sadiq et al. (Sadiq et al., 2022) determined the slip-flow conditions passing on the disk spiraling with simultaneous radial rotation/stretching of bulk Jeffrey fluid. Khan et al. (Khan et al., 2022) studied the temperature and velocity slip conditions, which are attached by using the mathematical model of Maxwell hybrid nanofluid. Many scholars (Li et al., 2021; Khan et al., 2021; Alreshidi et al., 2020) presented the comprehensive studies related to the velocity slip with hybrid Darcy-Forchheimer nano liquid, heat transfer in tangent hyperbolic fluid and magnetohydrodynamics (MHD) nanofluid flow through a porous rotating disc.

The mechanisms of force and natural convection work together with the heat transfer in the fluid, which is known as mixed convection. Alternatively, the flow, temperature, geometry, and direction play a significant role of convection contributes using the heat transfer. In very high-power devices, the forced convection is insufficient to complete the heat dissipation along with the combination of natural and forced convection. Few more investigations related to the mixed convection in the nanofluid are presented in (Kumar et al., 2022). Mixed convection analysis along with the non-uniform heat sink/source is discussed by Irfan et. al (Irfan et al., 2022). Gautam et. al (Gautam et al., 2020) performed the analysis related to the flow of MHD boundary using the non-Newtonian fluid with Soret/Dufour effects. Furthermore, the mixed convective three-dimensional (3D) nano-liquid flow using different facts are presented in these references (Alghamdi, 2020; Awan et al., 2022).

Cross fluid is a significant subclass of generalized Newtonian fluids. However, these kinds of fluids are actually non-Newtonian in nature. The primary characteristic of these fluids shows the dependence on the shear rates based on the viscosity. The properties of generalized Newtonian fluids are evaluated through different variations in fluid flow behaviour. To overcome these constraints, the Cross model first time is used which is presented in 1965 (Cross, 1965). At very high/low shear rate, the fluid's pseudoplastic and dilatant properties can be described using this model. The Cross modelling is implemented in various engineering systems due to the time characteristic (Khan et al., 2017). Ayub et al. (Ayub et al., 2022) used two rotating disks to compute the homogeneous/heterogeneous and Lorentz force impacts using 3D radiative Cross nanofluid. Hosseinzadeh et. al (Corke and Knasiak, 1998) investigated the Cross-fluid flow with nanoparticles of gyrotactic microorganisms' past on the cylinder. Cross fluid flow along with the irreversibility analysis and the Carboxymethyl cellulose water mixture using the hybrid nanofluid is discussed by Ali et. al (Hosseinzadeh et al., 2020). The Cross fluid is studied in various applications that are discussed in these references (Ali et al., 2023; Anjum et al., 2023). The study of the Cross fluid has been presented in various application in recent literature (Ayub et al., 2022; Ayub et al., 2021; Ayub et al., 2022; Shah et al., 2021). In these studies, the relation of bioconvection and Cross-diffusion effects is carried out by using the analysis of Cross fluid.

1.1. Motivation

The study of inclined magnetized unsteady Cross flow with attached buoyancy effects and energy loss over the coated disks is used to understand and predict the behavior of different flows in various industry and renewable energy systems. In many cooling and heat exchangers processes, the flow of fluid is often affected by the buoyancy forces due to the temperature gradients. Similarly, in the systems of renewable energy, such as solar thermal systems, the flow of fluid is affected by the buoyancy forces due to the presence of heat source. Additionally, many industrial processes involve the use of magnetic fields, such as heating and magnetohydrodynamic power generation. To understand the combined effects of buoyancy, magnetic fields, and energy loss is used due to the flow coatings characteristics, which is crucial to design and optimize these systems. This study aims to provide the valuable insights using these effects and contribute to the ongoing research in the field.

1.2. Novelty

The current study represents the novel contributions using the comprehensive analysis of an inclined magnetized unsteady Cross flow over a coated disk with attached buoyancy effects and energy loss. To the best of our knowledge, there has been limited research on the combined effects of buoyancy, magnetic fields, and energy loss due to coatings on the flow characteristics in this specific context. Furthermore, this study presents the numerical simulations of the governing equations, which provides a more accurate and detailed analysis of the flow characteristics as compared to previous studies, which have been calculated through the analytical or experimental methods. Additionally, this study focuses on the effects of the inclination angle, magnetic field strength, and coating thickness using the flow characteristics and energy loss, which provides a depth understanding based on these effects. Overall, this study provides a new and unique perspective on the behavior of inclined magnetized unsteady Cross flows with attached buoyancy effects and energy loss over the coated disks.

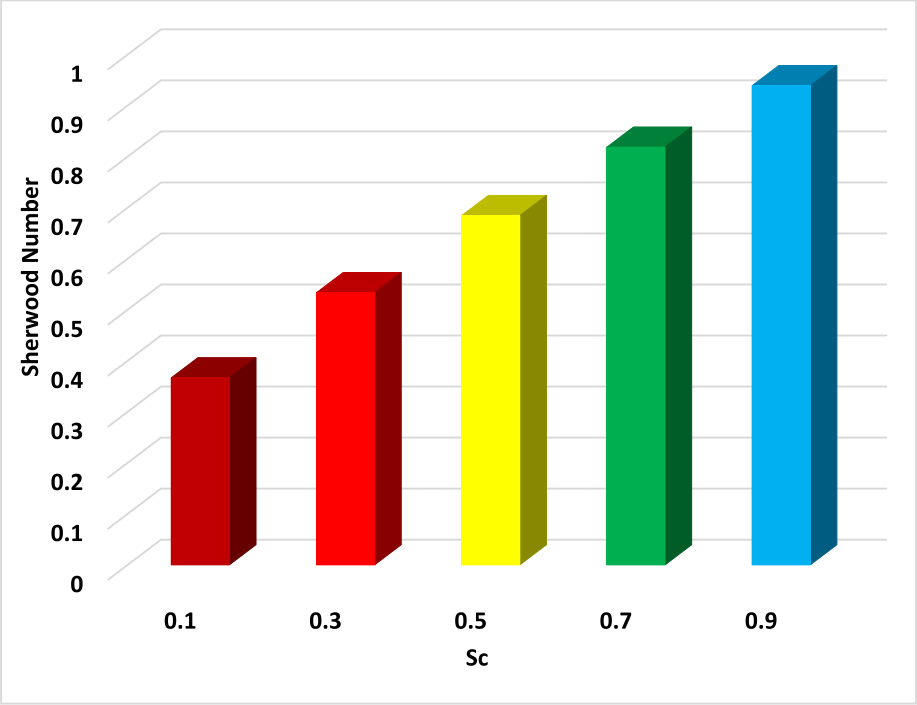

Chart 1 Brief review of the mathematical model.

Rest of the paper is summarized as: Section 2 presents the method and material, Section 3 shows the results and discussions, Section 4 indicates the conclusions.

2. Method and material

Under the influence of gentle force and dense scattering, the incompressible unsecure diffusive connective unstable advancements of the Carreau fluid (CF) past on a covered disk were observed. The disks straight line velocity $\left(\upsilon = \frac{cr}{l}\right)$ is accountable for evolving the axisymmetric flimsy stream of CF in the consequence of covering system. $\widetilde{T}_w$ and $\widetilde{T}_\infty$ represent the conducting disk and fluid surface temperature, while $\widetilde{C}_w$ and $\widetilde{C}_\infty$ represent the disk and fluid concentrations. The stream calculation using the *rz*-plane is presented in Fig. 1.

The accompanying velocity capability is applied for the axisymmetric fluid flow as:

$$V = \bar{u}(t,r,z)e_r + \bar{w}(t,r,z)e_z \tag{1}$$

In the above Eq. (1), $\bar{w}$ and $\bar{u}$ represent the axial and circular velocities. The energy, velocity, and concentration conditions using the blended diffusive progression based on the CF are assumed as:

$$div V^* = 0 \tag{2}$$

$$\rho\left(\frac{\partial V}{\partial t} + (V^*.\nabla)V^*\right) = div\,\tau + F^*, \tag{3}$$

F^* is defined as:

$$F^* = \left\{\beta_{\widetilde{C}}\left(\widetilde{C} - \widetilde{C_\infty}\right) + \beta_{\widetilde{T}}\left(\widetilde{T} - \widetilde{T_\infty}\right)\right\}g\rho, \tag{4}$$

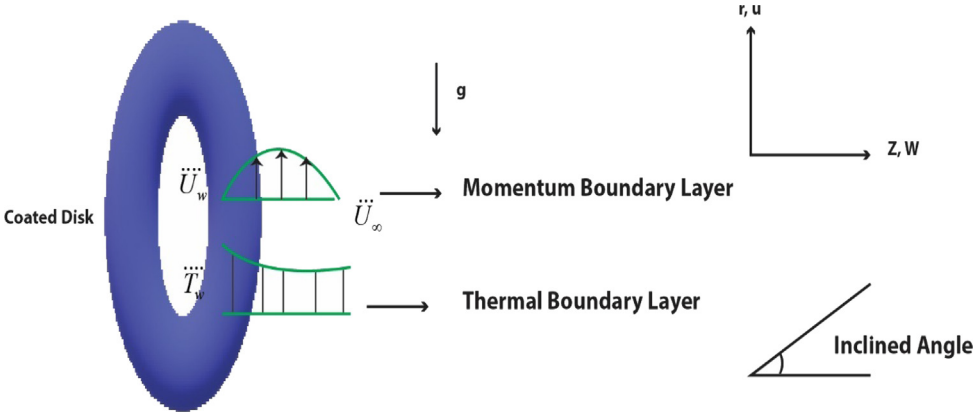

Fig. 1 Configuration of fluid analysis in the inclined magnetized environment.

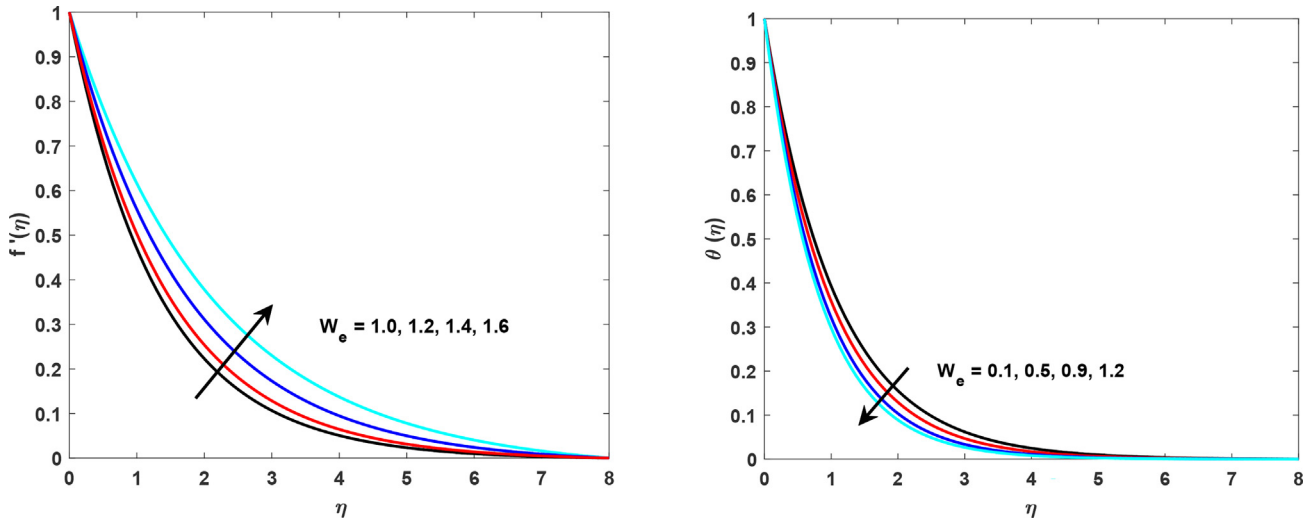

Fig. 2 **(a, b)**: Represents the values of Weissenberg number *(We)* on speed and temperature profiles.

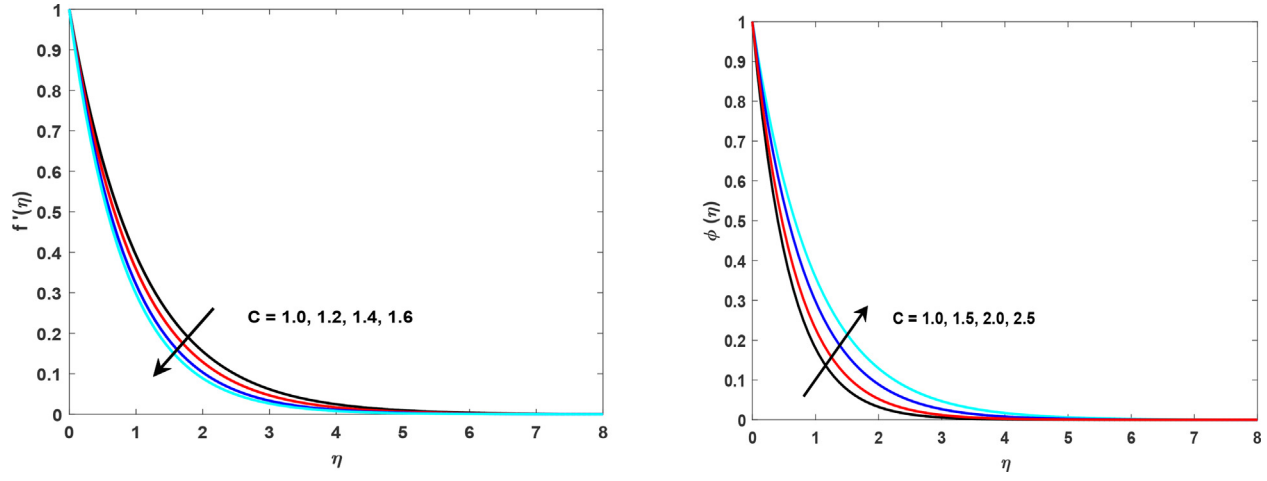

Fig. 3 **(a, b)** Different values of C on velocity and concentration profile.

$$\tau = -pI + \widetilde{\eta} A_1,\ A_1 = L^{\widetilde{T}} + L,\quad L = grad\, V^* \tag{5}$$

$$\widetilde{\eta} = \widetilde{\eta_\infty} + (\widetilde{\eta_o} - \widetilde{\eta_\infty})\left[\frac{1}{1+\left(\widetilde{\Gamma}\dot{r}\right)^n}\right], \rho\widetilde{C_\rho}\left(\frac{\partial \widetilde{T}}{\partial t} + (\nabla . V^*)\widetilde{T}\right) = r\nabla^2 \bar{T} + \mu^* trace(A_1 L) \tag{6}$$

$$\frac{\partial \widetilde{C}}{\partial t} + (V^* . \nabla)\widetilde{C} = D\left(\nabla^2 \widetilde{C}\right) \tag{7}$$

The boundary and initial conditions are presented as fallows

$$\widetilde{u} = U_w,\ \widetilde{w} = o,\ \widetilde{T} = \widetilde{T}_w, \widetilde{C} = \widetilde{C}_w \quad at\ z = 0, \tag{8a}$$

$$\widetilde{u} \to 0,\ \widetilde{T} = \widetilde{T}_w, \widetilde{C} = \widetilde{C}_w\, as\ z \to \infty \tag{8b}$$

$$\widetilde{u} = 0,\ \widetilde{T} = 0,\ \widetilde{C} = 0,\ \widetilde{w} = 0,\ at\ t = 0, \tag{8c}$$

In the above equation, $\left(U_w = \frac{cr}{t}\right)$ represents the coated disk rapidity, a is the thermal conductivity, $\beta_{\widetilde{C}}$ illustrates the concentration extension parameter, $\widetilde{\eta_\infty}$ represents the viscosity based on infinite shear-rate, η^{**} shows the Cross fluid viscosity, $\widetilde{T}_\infty$ and $\widetilde{C}_\infty$ present the ambient temperature and concentration, β_T describes the thermal extension parameter, $\eta_\circ$ represents the viscosity based zero shear-rate, $\widetilde{C}_w$ and $\widetilde{T}_w$ are the concentration and wall temperature. Subsequently, the accompanying boundary layer are presented in conditions (2–8) shows the conditions (9–13)

$$\widetilde{w} = o(\delta),\ r = o(1),\ \widetilde{C} = o(1),\ \widetilde{z} = o(\delta),$$
$$\widetilde{w} - o\left(\delta^2\right),\ t = o(1),\ \Gamma = o\left(\delta^2\right),\ \widetilde{T} = o(1),$$

$$\frac{\widetilde{u}}{r} + \frac{\partial \widetilde{u}}{\partial r} = -\frac{\partial \widetilde{u}}{\partial z} \tag{9}$$

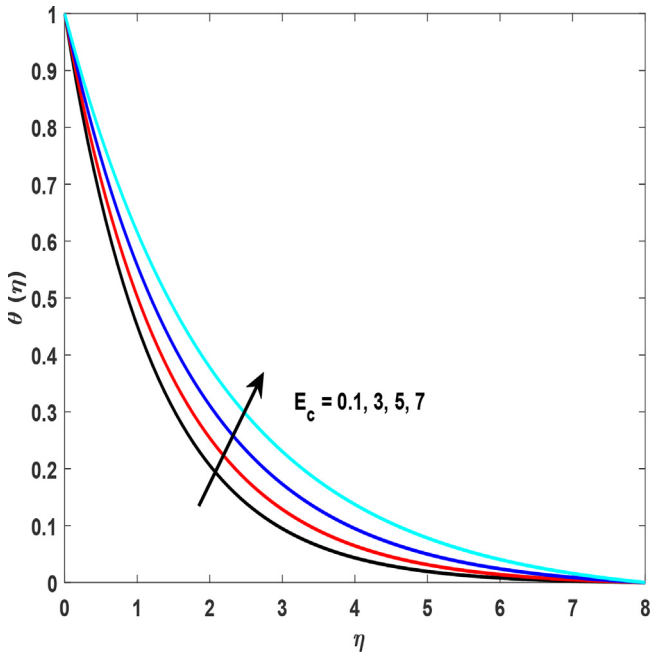

Fig. 4 Represents the Eckert number on temperature profile.

$$\frac{\partial \widetilde{u}}{\partial t}+\widetilde{u}\frac{\partial \widetilde{u}}{\partial r}+\widetilde{w}\frac{\partial \widetilde{u}}{\partial z} - \left\{g\beta_{\widetilde{C}}\left(\widetilde{C}-\widetilde{C_\infty}\right)+g\beta_{\widetilde{T}}\left(\widetilde{T}-\widetilde{T_\infty}\right)\right\} = \upsilon\frac{\partial}{\partial z}\left[\left\{1+\Gamma^2\left(\frac{\partial \widetilde{u}}{\partial z}\right)\right\}^{-1}\frac{\partial \widetilde{u}}{\partial z}\right], \tag{10}$$

$$\frac{\partial \widetilde{T}}{\partial t}+\widetilde{u}\frac{\partial \widetilde{T}}{\partial r}+\widetilde{w}\frac{\partial \widetilde{T}}{\partial z}=\frac{k}{\rho\widetilde{C}_\rho}\frac{\partial^2\widetilde{T}}{\partial z^2}+\frac{\upsilon}{\widetilde{C}_\rho}\left[\frac{\left(\frac{\partial \widetilde{u}}{\partial z}\right)^2}{1+\left(\Gamma\left(\frac{\partial \widetilde{u}}{\partial z}\right)\right)^n}\right], \tag{11}$$

$$\frac{\partial \widetilde{C}}{\partial t}+\widetilde{u}\frac{\partial \widetilde{C}}{\partial r}+\widetilde{w}\frac{\partial \widetilde{C}}{\partial z}=D\frac{\partial^2\widetilde{C}}{\partial z^2}. \tag{12}$$

$$at\ \ \widetilde{z}=0,\ \ U=\frac{cr}{t},\ \widetilde{w}=0,\ \widetilde{T}=\widetilde{T_w},\ \widetilde{C}=\widetilde{C_w}$$

The following conditions are given as:

$$at\ \widetilde{z}=0,\ \ \widetilde{w}=0,\ U=\frac{cr}{t},\widetilde{T}=\widetilde{T_w},\ \widetilde{C}=\widetilde{C_w} \tag{13a}$$

$$at\ \widetilde{t}\to\infty,\widetilde{C}=\widetilde{C_\infty},\ \ U\to 0,\ \ \widetilde{T}=\widetilde{T_w}, \tag{13b}$$

$$at\ t=\ \widetilde{u}=\ \widetilde{w}=\ \widetilde{T}=\ \widetilde{C}=0. \tag{13c}$$

The non-layered factors are given as:

$$\widetilde{\eta}=\sqrt{\frac{c}{\widetilde{\nu}t}}z,\ \ \theta=\frac{\widetilde{T_\infty}-\widetilde{T}}{\widetilde{T_\infty}-\widetilde{T_w}},\ \widetilde{u}=\frac{cr}{t}\widetilde{f}'(\eta),\widetilde{w} =-2\frac{\sqrt{c\upsilon}}{t}\widetilde{f}(\eta),\phi=\frac{\widetilde{C}-\widetilde{C_\infty}}{\widetilde{C_w}-\widetilde{C_\infty}}, \tag{14}$$

The above Eq is used in conditions (9) to (13), the obtained framework is acquired as:

$$\left[2\widetilde{f}''\widetilde{f}-\left(\widetilde{f}'\right)^2+\lambda(\theta+N_r\phi)+\frac{1}{c}\left(\widetilde{f}'-\frac{\eta}{2}\widetilde{f}''\right)\right]\left\{1+\left(We\widetilde{f}''\right)^n\right\}^{-2} +\left\{1+(1-n)\left(We\widetilde{f}''\right)^n\right\}\widetilde{f}''' =0, \tag{15}$$

$$\mathrm{Pr}\theta''+2\theta'\widetilde{f}+\frac{\eta}{2c}\theta'+Ec\left(\widetilde{f}''\right)^2\left(\left(We\widetilde{f}''\right)^n+1\right)^{-1}=0, \tag{16}$$

$$\phi''+\left(2\widetilde{f}''\phi'+\frac{\eta}{2c}\phi'\right)Sc=0 \tag{17}$$

$\widetilde{f}(0)=0,\ \widetilde{f}'(0)=\theta(0)=1$, The above issue decreases using the flow of boundary layer when $We,\lambda\to 0$. Additionally, energy decreasing impacts can be noticed through Eckert number. Boundary conditions are presented as:

$$\widetilde{f}(0)=0,\ \widetilde{f}'(0)=\theta(0)=\phi(0)=1, \tag{18a}$$

$$\widetilde{f}'(\infty),\theta(\infty)\&\phi(\infty)\to 0 \tag{18b}$$

Weissenberg number is $\left(We=\Gamma cr\sqrt{\frac{c}{\widetilde{\nu}t}}/t\right)$, the parameter of buoyancy ratio is $\left(N_r=\frac{\beta_{\widetilde{C}}\left(\widetilde{C_w}-\widetilde{C_\infty}\right)}{\beta_{\widetilde{T}}\left(\widetilde{T_w}-\widetilde{T_\infty}\right)}\right)$, $\left(Ec=\frac{U(r)}{\widetilde{T_\infty}\widetilde{C_\rho}}\right)$ is the Eckert number, $\left(\lambda=\frac{g\beta_{\widetilde{T}}\left(\widetilde{T_w}-\widetilde{T_\infty}\right)r}{(U_w)^2}\right)$ represents the buoyancy parameter, $(Sc=\upsilon)$ and $\left(\mathrm{Pr}=\frac{\eta\circ\widetilde{C_\rho}}{k}\right)$ are the is called Schmidt and Prandtl numbers. Local skin-friction coefficient (SFC) is $\widetilde{C_\rho}$, local Nusselt number (LNN) is Nu, and Sherwood number (SN) is S_h are given as:

$$\widetilde{C_\rho}=\frac{\tau_{rz}|_z=0}{\frac{1}{2}U_{2\rho}} \tag{19}$$

where

$$\tau_{rz}|_{z=0}=\left[\widetilde{\eta}_\circ\frac{\widetilde{u_z}}{\{\Gamma\widetilde{u_z}\}^n+1}\right]_{\widetilde{z}=0} \tag{20}$$

The SFC with dimensionless formulation is given as:

$$\frac{1}{2}\sqrt{Re}\,\widetilde{C}_f=-\frac{\widetilde{f}''(0)}{1+\left(\widetilde{f}''(0)We\right)^n} \tag{21}$$

The LNN is presented as:

$$Nu=\frac{r\widetilde{q_w}}{k\left(\widetilde{T_w}-\widetilde{T_\infty}\right)'} \tag{22}$$

Where $\left(\widetilde{q_w}=-kT_{\widetilde{z}}|_{\widetilde{z}=0}\right)$ represents the surface heat flux. The dimension less LNN is shown as:

$$\frac{Nu}{\sqrt{Re}}=-\theta'(0) \tag{23}$$

SN is expressed as:

$$Sh=\frac{r\widetilde{q_c}}{D\left(\widetilde{C_w}-\widetilde{C_\infty}\right)'} \tag{24}$$

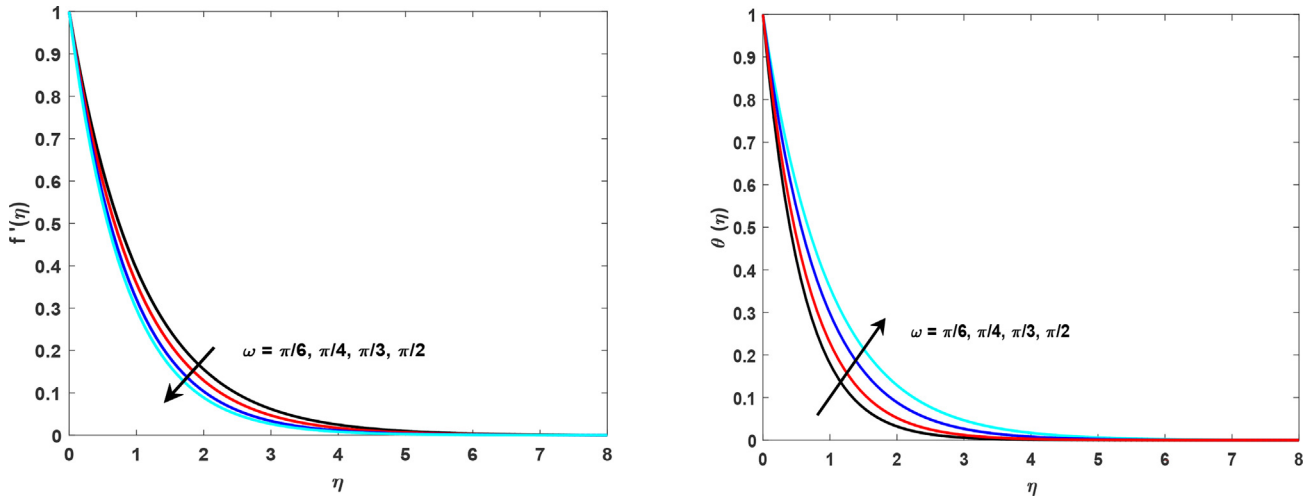

Fig. 5 **(a, b).** Different values of inclined angle on velocity and temperature profile.

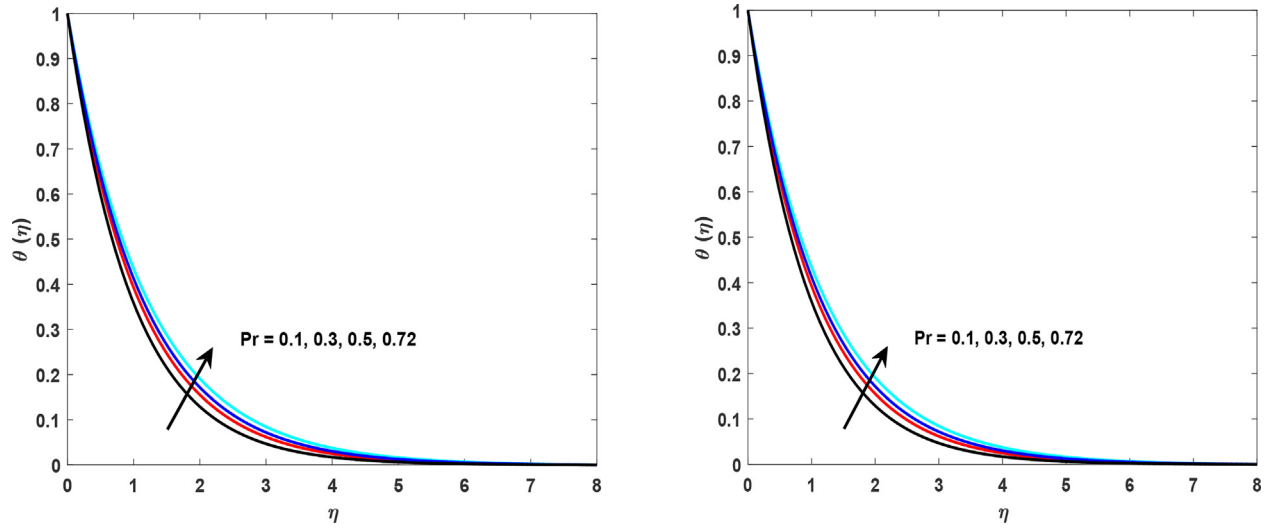

Fig. 6 **(a, b)** Representations the Pr on velocity and temperature state.

In Eq. (24), $\left(\widetilde{q_c} = -D\widetilde{C_c}|_{\widetilde{z}=0}\right)$ represents the flux of surface mass, and SN is defined as:

$$\frac{Sh}{\sqrt{Re}} = -\phi'(0) \tag{25}$$

The arrangement of exceptionally conditions (15) to (17) are tackled by approximate solution, the shooting method, which is a simple and proficient technique for calculations. The MATLAB is used for the computational examinations based on the shooting technique, which is depicted as:

$$y_1 = \widetilde{f},\ y_2 = \widetilde{f}',\ y_3 = \widetilde{f}'' \tag{26}$$

$$y_3' = \widetilde{f}''' = -\frac{\left[1 + (Wey_3)^n\left[2y_1y_3 - y_2^2 + \frac{1}{c}\left(y_2 - \frac{\eta}{2}y_3\right) + \lambda(N_r y_6 + y_4)\right]\right]}{[1 + (Wey_3)^n(1-n)]} \tag{27}$$

$$y_4 = \theta,\ y_5 = \theta' \tag{28}$$

$$y_5' = \theta'' = -\frac{1}{\Pr}\left[2y_1y_5 + \frac{\eta}{2c}y_5 + \frac{Ecy_3^2}{(1 + (Wey_3)^n)}\right] \tag{29}$$

$$y_6 = \varphi,\quad y_7 = \varphi' \tag{30}$$

$$y_7' = \varphi'' = -Sc\left(2y_1y_7 + \frac{\eta}{2c}y_7\right) \tag{31}$$

With the initial conditions

$$y_1(0) = 0,\ y_1'(0) = 1, y_4(0) = 1,\ y_6(0) = 1 \tag{32}$$

3. Results and discussion

In this section, the details of the numerical results and discussions are performed of the system of differential equations. Chart 1 shows the problem description of the problem.

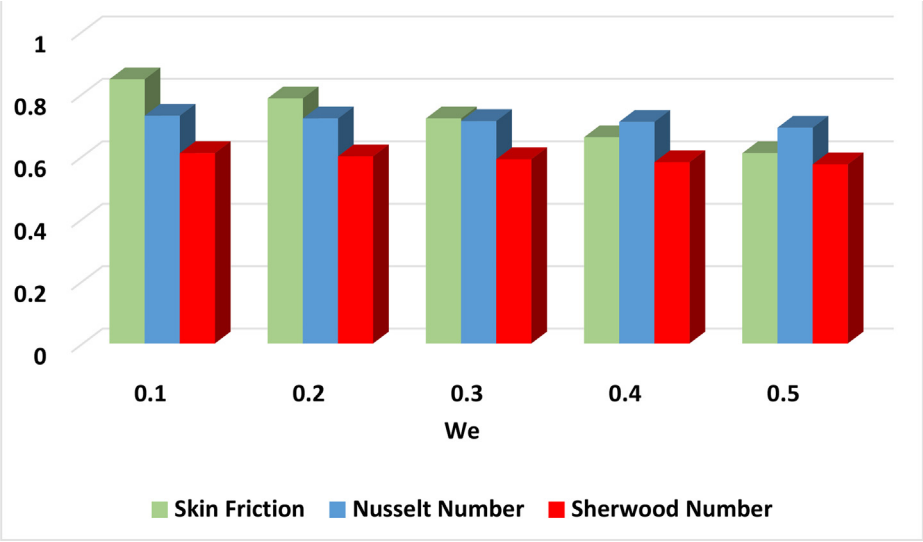

Fig. 7 LSF, LNN and SN using the values of *We*.

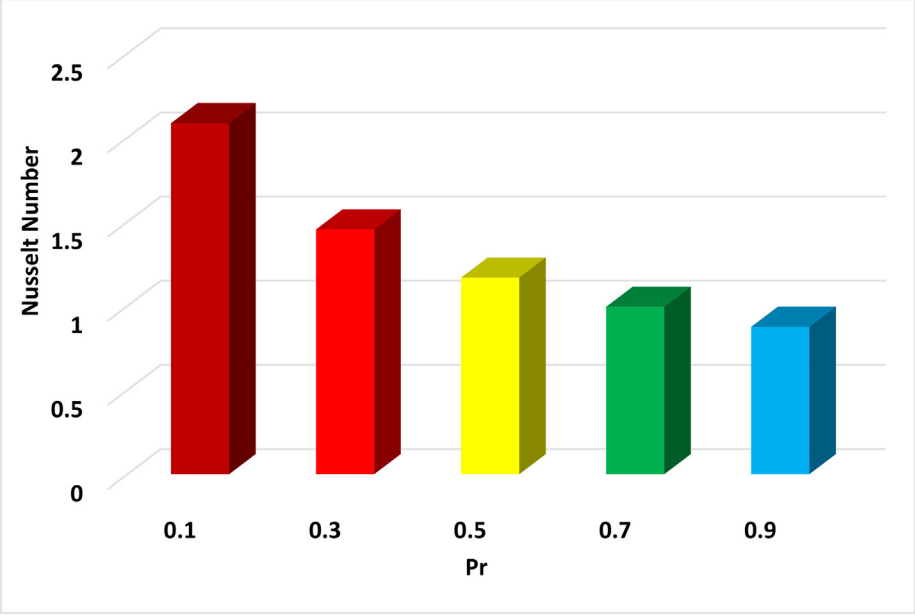

Fig. 8 Pr with Nusselt number.

In the light of the fact that the moving surface results in a decline, which regulates the Cross CF flow using the boundary layer. Fig. 2 addresses the boundary layer velocity horizontally along the circle drops with the rising upsides of the Cross-fluid velocity boundary-based surface level. This figure shows that the outcomes for the arbitrary upsides of the Weissenberg number (*We*) by fixing different boundaries appeared as the above ordinary differential equation. "*We*" contains the time relaxation steady terms along with the impacts of velocity and temperature. Fig. 2a and Fig. 2b address the various upsides of *We* based on the profile of speed and temperature. Fig. 2a illustrates that by expending the upsides of *We*, speed profile builds because of shear diminishing / thickening area of Cross fluid. It is demonstrated that *We* shows the shear reducing influences, which weaken the resistive powers in the Cross CF. The velocity of Cross fluid past over the surfaces increases with an increase in *We* using the boundary area. The rising impacts of bouncy ratio parameters lightness the percentage due to the concentration that is addresses in Fig. 3. Temperature of CF heightens with mounting upsides of the Eckert number addresses in Fig. 4. Different nonlinear dimensionless boundaries diagrams in view of temperature, velocity and concentration profiles are given in Figs. 2 to 6. Figs. 5 to 9 indicate the expanding form of the activation energy parameters and

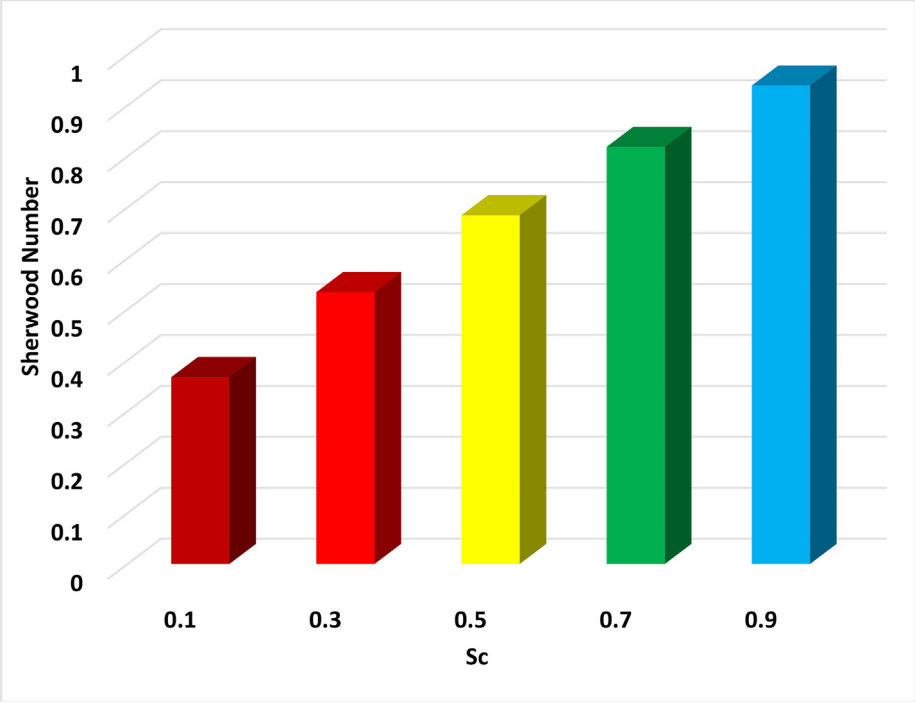

Fig. 9 Schmidt number on SN.

Table 1 Approximate results of LSF, LNN and SN for n = 1, Pr = 0.7, c = 5, Ec = 0.2, l = 0.1, Sc = 0.2, and Nr = 1.

We	LSF	LNN	SN
0.1	0.84565493	0.7290323	0.6089283
0.2	0.78450391	0.7200034	0.5987382
0.3	0.72003922	0.7118328	0.5892892
0.4	0.65990943	0.7092092	0.5800029
0.5	0.60874521	0.6903284	0.5729384

Table 2 Pr impacts on LNN using n = 2, We = 0.2, Ec = 0.2, l = 0.1, Sc = 0.2, c = 5, and Nr = 1.

Pr	LNN
0.1	2.0853235
0.3	1.4543438
0.5	1.1674382
0.7	0.9942291
0.9	0.8752134

Table 3 Effect of *Sc* on SN for $n = 2$, $We = 0.2$, $Ec = 0.2$, $l = 0.1$, $Pr = 0.7$, $c = 5$ and $Nr = 1$.

Sc	SN
0.1	0.3665143
0.3	0.5333454
0.5	0.6843373
0.7	0.8185223
0.9	0.9389392

response rate boundary nano-molecule velocity profile improved and devaluated. Fig. 5a presents the shear diminishing area of Cross fluid, axial component, and temperature, which are directly related to each other. Fig. 5b indicates the shear thickening space of Cross fluid that unveil the similar way of behaving. Axial components and normal temperature depend upon on each other. Obviously by developing the upsides of n, the speed and temperature profiles reduce. As $K\alpha.\frac{1}{R}$ is used to expand the curvature parameter range of tubed shaped surface that lessons the fluid contact with surface diminishes and less obstruction along these fluid particles in the boundary layer. The variety in CF particles temperature regarding involved boundary in the sight of definition ($S = 0.2$) and in the non-appearance of ($S = 0.0$) are clarified with the assistance of Fig. 6a and 6b. Witness the diminishing way of behaving the thermal distribution because of moderate extent of Pr layer and non-stratification. This conduct is legitimated is presence of converse convection of Pr and thermal energy diffusion. Fig. 6a addresses the values of Pr on the velocity profile, while Fig. 6b represents the performances of Pr on the temperature profile.

3.1. Aspect of physical interpretation

In this analysis, the coefficients of LSF, LNN, and SN for various boundary layers in Table 1. By expanding the magnetic parameter, LSF coefficient increases, while LSF and SN reduces. It is seen that by expanding the response rate of the

boundary, Nusselt number and Skin fraction coefficient does not change, while Sherwood number increases.

Graphical impact of unsteadiness (parameter) axial component on different profiles

From the graphical representations, it is observed that if Pr and K increases then the LNN declined mentality. By increasing LNN, magnetic parameter reduces. The justification for improvement the size of intensity move rate shows the increment in Pr, which represents the proportion between energy to warm diffusivity express by Pr. By expanding Pr, energy diffusivity improves, and normal motor movement of liquid particles attaches that shows the expansion in the intensity move rate. Moreover, the variety showed by different boundaries on LSF and LNN are likewise justifiable using the information of Tables 1 and 2. Table 1 portrays the mathematical variety in coefficient of drag force regarding We and attractive field boundary (M) for round/hollow and level surfaces (K = 0.5) and (K = 0.0). From the mathematical information it very well may be examined that wall shear pressure if there should arise an occurrence of level surface is clearer than chamber. (See Table 3).

4. Conclusions

The results of this study provide the valuable insights into the effects of buoyancy, magnetic field, and coating thickness on the flow characteristics and energy loss of an inclined magnetized unsteady Cross flow over a coated disk. The numerical simulation method used in the study has been proven to be an accurate and reliable way to predict the fluid flow and energy loss in the system. The study could have practical applications in the design and optimization of systems that involve buoyancy-driven flows in the presence of magnetic fields, such as in various industrial processes and renewable energy systems.

Conclusion is summarized in points given as:

1. The buoyancy effect has a significant impact on the flow, resulting in an increase in the flow velocity.
2. The magnetic field also has a significant effect on the flow, with the velocity decreasing as the magnetic field strength increases.
3. The coating thickness has a significant effect on the energy loss, with the energy loss decreasing as the coating thickness increases.
4. The inclination angle has an effect on the flow characteristics and energy loss, with an increase in the angle leading to a change in the flow pattern and energy loss.

Declaration of Competing Interest

The authors declare that they have no known competing financial interests or personal relationships that could have appeared to influence the work reported in this paper.

References

Acharya, N., 2021. Spectral simulation to investigate the effects of nanoparticle diameter and nanolayer on the ferrofluid flow over a slippery rotating disk in the presence of low oscillating magnetic field. Heat Transfer 50 (6), 5951–5981.

Alghamdi, M., 2020. Significance of Arrhenius activation energy and binary chemical reaction in mixed convection flow of nanofluid due to a rotating disk. Coatings 10 (1), 86.

Ali, F., Kumar, T.A., Loganathan, K., Reddy, C.S., Pasha, A.A., Rahman, M.M., Al-Farhany, K., 2023. Irreversibility analysis of cross fluid past a stretchable vertical sheet with mixture of Carboxymethyl cellulose water based hybrid nanofluid. Alex. Eng. J. 64, 107–118.

Alishiri, M., Ebrahimi, S., Shamloo, A., Boroumand, A., Mofrad, M. R., 2021. Drug delivery and adhesion of magnetic nanoparticles coated nanoliposomes and microbubbles to atherosclerotic plaques under magnetic and ultrasound fields. Eng. Appl. Comput. Fluid Mech. 15 (1), 1703–1725.

Alreshidi, N.A., Shah, Z., Dawar, A., Kumam, P., Shutaywi, M., Watthayu, W., 2020. Brownian motion and thermophoresis effects on MHD three dimensional nanofluid flow with slip conditions and Joule dissipation due to porous rotating disk. Molecules 25 (3), 729.

Anjum, N., Khan, W.A., Azam, M., Ali, M., Waqas, M., Hussain, I., 2023. Significance of bioconvection analysis for thermally stratified 3D Cross nanofluid flow with gyrotactic microorganisms and activation energy aspects. Therm. Sci. Eng. Prog. 38, 101596.

Awan, F.J., Maqbool, K., Sait, S.M., Ellahi, R., 2022. Buoyancy effect on the unsteady diffusive convective flow of a Carreau fluid passed over a coated disk with energy loss. Coatings 12 (10), 1510.

Ayub, A., Wahab, H.A., Shah, S.Z., Shah, S.L., Darvesh, A., Haider, A., Sabir, Z., 2021. Interpretation of infinite shear rate viscosity and a nonuniform heat sink/source on a 3D radiative cross nanofluid with buoyancy assisting/opposing flow. Heat Transfer 50 (5), 4192–4232.

Ayub, A., Sabir, Z., Shah, S.Z.H., Wahab, H.A., Sadat, R., Ali, M.R., 2022. Effects of homogeneous-heterogeneous and Lorentz forces on 3-D radiative magnetized cross nanofluid using two rotating disks. Int. Commun. Heat Mass Transfer 130, 105778.

Ayub, A., Sabir, Z., Altamirano, G.C., Sadat, R., Ali, M.R., 2022. Characteristics of melting heat transport of blood with time-dependent cross-nanofluid model using Keller-Box and BVP4C method. Eng. Comput. 38 (4), 3705–3719.

Corke, T.C., Knasiak, K.F., 1998. Stationary travelling cross-flow mode interactions on a rotating disk. J. Fluid Mech. 355, 285–315.

Cross, M.M., 1965. Rheology of non-Newtonian fluids: a new flow equation for pseudoplastic systems. J. Colloid Sci. 20 (5), 417–437.

Dandapat, B.S., Singh, S.K., 2015. Unsteady two-layer film flow on a non-uniform rotating disk in presence of uniform transverse magnetic field. Appl. Math Comput. 258, 545–555.

Dickey, J. M., West, J., Thomson, A. J., Landecker, T. L., Bracco, A., Carretti, E. T. T. O. R. E., ... & Wolleben, M. (2022). Structure in the magnetic field of the milky way disk and halo traced by faraday rotation. *The Astrophysical Journal*, *940*(1), 75.

Gautam, A.K., Verma, A.K., Bhattacharyya, K., Banerjee, A., 2020. Soret and Dufour effects on MHD boundary layer flow of non-Newtonian Carreau fluid with mixed convective heat and mass transfer over a moving vertical plate. Pramana 94, 1–10.

Hosseinzadeh, K., Roghani, S., Mogharrebi, A.R., Asadi, A., Waqas, M., Ganji, D.D., 2020. Investigation of cross-fluid flow containing motile gyrotactic microorganisms and nanoparticles over a three-dimensional cylinder. Alex. Eng. J. 59 (5), 3297–3307.

Hu, L., Wang, N., Lim, Y.D., Miao, J., 2020. Chemical reaction dependency, magnetic field and surfactant effects on the propulsion of disk-like micromotor and its application for E. coli transportation. Nano Select 1 (4), 432–442.

Irfan, M., Sunthrayuth, P., Ali Pasha, A., Anwar, M.S., Azeem Khan, W., 2022. Phenomena of thermo-sloutal time's relaxation in mixed convection Carreau fluid with heat sink/source. Waves Random Complex Media, 1–13.

Khan, W., Badruddin, I.A., Ghaffari, A., Ali, H.M., 2021. Heat transfer in steady slip flow of tangent hyperbolic fluid over the lubricated surface of a stretchable rotatory disk. Case Stud. Therm. Eng. 24, 100825.

Khan, M., Manzur, M., ur Rahman, M., 2017. On axisymmetric flow and heat transfer of Cross fluid over a radially stretching sheet. Results Phys. 7, 3767–3772.

Khan, U., Zaib, A., Waini, I., Ishak, A., Sherif, E.S.M., Xia, W.F., Muhammad, N., 2022. Impact of Smoluchowski temperature and Maxwell velocity slip conditions on axisymmetric rotated flow of

hybrid nanofluid past a porous moving rotating disk. Nanomaterials 12 (2), 276.

Kumar, A., Ray, R.K., Sheremet, M.A., 2022. Entropy generation on double-diffusive MHD slip flow of nanofluid over a rotating disk with nonlinear mixed convection and Arrhenius activation energy. Indian J. Phys., 1–17

Li, Y.X., Muhammad, T., Bilal, M., Khan, M.A., Ahmadian, A., Pansera, B.A., 2021. Fractional simulation for Darcy-Forchheimer hybrid nanoliquid flow with partial slip over a spinning disk. Alex. Eng. J. 60 (5), 4787–4796.

Naveed Khan, M., Ahmad, S., Ahammad, N.A., Alqahtani, T., Algarni, S., 2022. Numerical investigation of hybrid nanofluid with gyrotactic microorganism and multiple slip conditions through a porous rotating disk. Waves Random Complex Media, 1–16.

Ray, P.C., Dandapat, B.S., 1994. Flow of thin liquid film on a rotating disk in the presence of a transverse magnetic field. Quart. J. Mech. Appl. Math. 47 (2), 297–304.

Sadiq, M.N., Sajid, M., Javed, T., Ali, N., 2022. Modeling and simulation for estimating thin film lubrication effects on flow of Jeffrey liquid by a spiraling disk. Eur. J. Mech.-B/Fluids 91, 167–176.

Shah, S.Z.H., Ayub, A., Sabir, Z., Adel, W., Shah, N.A., Yook, S.J., 2021. Insight into the dynamics of time-dependent cross nanofluid on a melting surface subject to cubic autocatalysis. Case Stud. Therm. Eng. 27, 101227.

Shuaib, M., Shah, R. A., & Bilal, M. (2020). Variable thickness flow over a rotating disk under the influence of variable magnetic field: An application to parametric continuation method. *Advances in Mechanical Engineering*, *12*(6), 1687814020936385.